

Plasmonischer Beitrag zur Casimir-Kraft zwischen zwei Lagen Graphen

zur Erlangung des akademischen Grades
Bachelor of Science
(B.Sc.)
im Fach Physik



eingereicht an der
Mathematisch-Naturwissenschaftlichen Fakultät
Institut für Physik
Humboldt-Universität zu Berlin

von
Christoph Heiko Egerland
geboren am 14.03.1996 in Plauen

Gutachter:

1. *Prof. Dr. Kurt Busch*
2. *Prof. Dr. Oliver Benson*

Ich erkläre hiermit, dass ich die vorliegende Arbeit, unter Beachtung der Prüfungsordnung für das Bachelorstudiums Physik vom 31.07.2014, selbstständig verfasst und noch nicht für andere Prüfungen eingereicht habe. Sämtliche Quellen einschließlich Internetquellen, die unverändert oder abgewandelt wiedergegeben werden, insbesondere Quellen für Texte, Grafiken, Tabellen und Bilder, sind als solche kenntlich gemacht. Mir ist bekannt, dass bei Verstößen gegen diese Grundsätze ein Verfahren wegen Täuschungsversuchs bzw. Täuschung eingeleitet wird.

Berlin, den 13.11.2017

Übersicht

Diese Arbeit beschäftigt sich mit der Frage: “Welchen Einfluss haben plasmonische Moden auf den Casimir Effekt in Graphen?”. Hierfür beschreiben wir zunächst Graphen als Struktur mathematisch und untersuchen die Bandstruktur im Rahmen der Theorie stark gebundener Elektronen. Wir finden heraus, dass die Energiedispersion nahe der Bandlücke linear ist und folgern, dass die elektrooptischen Eigenschaften von Graphen im Bereich kleiner Energien (wenige eV) gut von einem (2+1)-dimensionalen Diracmodell beschrieben werden können. Aus diesem Modell erhalten wir die Reflektionskoeffizienten von Graphen, die wir für die weiteren Berechnungen benötigen. Des Weiteren vergleichen wir das Diracmodell mit dem Plasmamodell, welches zur Beschreibung des Casimireffektes in Graphen in der Literatur oft benutzt wurde. Nach einem kurzen Abriss über die Geschichte der Theorie zum Casimireffekt führen wir einen Ausdruck für die Casimirenergie zwischen zwei Lagen undotiertem Graphen bei null Temperatur, aber mit einer nicht verschwindenden Bandlücke ein und vergleichen diesen mit Ergebnissen für den Fall einer verschwindenden Bandlücke. Danach untersuchen wir die plasmonischen Moden für eine einzelne Lage Graphen, wobei sich herausstellt, dass nur eine in der sogenannten TE-Polarisation existiert. Im Falle von zwei zueinander parallelen Lagen Graphen koppeln die individuellen plasmonischen Moden symmetrisch oder antisymmetrisch. Wir finden heraus, dass die zu den Moden korrespondierenden Felder stets evaneszent, d.h. exponentiell an der Oberfläche abklingend, sind. Um den Beitrag plasmonischer Moden zum Casimireffekt zu bestimmen, führen wir die sogenannte plasmonische Energie ein, das heißt den Teil der Casimir Energie der aus den plasmonischen Moden resultiert. Für den Grenzfall verschwindender Abstände zwischen den beiden Metallplatten, wird die gesamte Casimirenergie beliebig groß. Besonders interessant ist hierbei, dass aus der Beschreibung von Graphen im Plasmamodell resultiert, dass die plasmonischen Moden für verschwindende Abstände ebenfalls beliebig groß werden und damit den Casimireffekt dominieren. Innerhalb unserer Betrachtung ist dies nicht zu bestätigen. Wir finden allerdings heraus, dass die plasmonische Energie für sehr kurze Abstände konstant wird. Für den Grenzfall sehr großer Abstände erhalten wir das gleiche Potenzgesetz, wie im Falle der Beschreibung Graphens mit dem Plasmamodell.

Introduction

In the framework of quantum mechanics the Heisenberg uncertainty principle states, that we can only measure at the same time position and momentum of a particle, within a fundamentally irreducible uncertainty. In quantum field theory the uncertainty principle manifests itself in intrinsic fluctuations of the fields, which have helped describe a lot of physical effects, such as the Lamb shift and the Hawking radiation. Although occurring at the microscopic scale, quantum fluctuations can lead to macroscopic effects, such as the Casimir force.

In this phenomenon two uncharged non-magnetic parallel plates, placed in the quantum vacuum, experience an attracting force. Usually negligible in everyday life, the Casimir force becomes very important if the two bodies are close to each other, i.e. with a distance in the micron or submicron regime. This occurs often in nanotechnologies, for example in a variety of systems called microelectromechanical systems (MEMS), which are microscopic devices made of movable components that are just some microns in size. They are already used as, e.g. inertial sensors in consumer electronics [1]. The Casimir force causes sticking between the MEMS' movable parts, but also promises to be used as a method of control. Beyond its application in MEMS, it is generally interesting to investigate the Casimir force in technologically relevant mechanical, electrical or optical systems. A favorable material, which, since its experimental isolation in 2004 [2], is of most interest to such devices is graphene. As the first truly two-dimensional material, graphene inhibits exotic features, such as a higher thermal conductivity than silver, whilst also being stronger than steel. In the literature, the optical properties of graphene have been studied using different models as, for example, the so called plasma model, where one describes the charge carriers in the layer as an incompressible two-dimensional electronic fluid. However, it has recently been shown that the plasma model predicts a too large magnitude of the Casimir force in graphene, whereas another model, the so called Dirac model, is in better agreement with the experimental data [3]. Other investigations on the Casimir effect, for the configuration of two parallel metal plates, have shown, that collective movements of charge carriers at the surface of the material, the so called surface plasmon polaritons, are of great importance for determining the Casimir force at small distances, i.e. where the attraction becomes largest [4]. Work on two two-dimensional plasma sheets have shown the same result, namely that surface plasmons dominate the Casimir interaction at small separations. Since this can be interpreted as a result for two interacting graphene layers, it is interesting to wonder whether this still holds or, in general, what happens in the case of the Dirac model, which seems to describe the Casimir interaction in graphene more truthfully. This issue is at the center of the present work.

We begin in Chapter 1 by introducing graphene mathematically and calculate its band structure using a tight-binding model. The Dirac model of graphene is then introduced, along with arguments describing its advantages with respect to the plasma model. We proceed in Chapter 2

by describing the derivation of the Casimir energy between two perfectly reflecting parallel plates, given by H.B.G. Casimir in 1948. We then show its generalization to dielectric materials and nonzero temperatures as proposed by Lifshitz in 1955. The Casimir energy for two graphene layers described by the Dirac model is calculated and compared to results found in the literature. In Chapter 3 we calculate the surface plasmons' dispersion relations for a single layer and two interacting layers of graphene and discuss their asymptotic expressions and their behaviour, in comparison to the results found for two metal plates. In Chapter 4 we calculate the plasmonic energy, which serves as a measure for the influence of plasmons in the Casimir effect. We evaluate the asymptotes in the limits of small and large separations between the graphene layers and compare the results to expressions found in the case of two interacting plasma sheets. Chapter 5 serves as a summary of our results.

Acknowledgments

I'd like to express my gratitude towards Prof. Dr. Kurt Busch and the whole TOP group for establishing the perfect surrounding for this thesis to be written in.

A special thanks goes to my supervisor Dr. Francesco Intravaia along with my co-supervisors Daniel Reiche and Marty Oelschläger for always helping me out, furthering my physical intuition, knowledge and generally creating a wholesome work space.

I also like to thank my cat Coco for always greating me with many purs after a long day at the MBI.

Thank You!

Contents

Übersicht	v
Introduction	vii
Acknowledgments	ix
1 Graphene	1
1.1 Crystal Structure	1
1.2 Tight-Binding Model	2
1.3 Electrooptical Properties	4
2 Casimir Energy	7
3 Plasmonic Modes Of Graphene	11
3.1 Single Layer Of Graphene	11
3.2 Two Layers Of Graphene	13
3.3 Parametrization	17
4 Plasmonic Energy	19
5 Summary	25
Bibliography	28

1

Chapter 1

Graphene

We introduce graphene as a two dimensional material and talk about its crystal structure and the resulting electronic properties, which we study in a tight-binding model. Within this framework we find a linear dispersion at the Dirac points, which enables us to study the optical properties of graphene via a (2+1)-dimensional Dirac model. As an overall result, we obtain the reflection coefficients.

1.1 Crystal Structure

Graphene can be described as a two-dimensional material that consists of carbon atoms arranged in a honeycomb crystal structure. More precisely, it is described as a hexagonal lattice with a two atom basis, which we call A and B in the following. For a comprehensive review see Ref. [5], whose notation we adopt for the present and following section.

We choose the z axis to be perpendicular to the graphene sheet, which is assumed to lay in the x-y-plane. The primitive lattice vectors between two unit cells are given by

$$\mathbf{a}_1 = \frac{a}{2} (1, \sqrt{3}) \quad \mathbf{a}_2 = \frac{a}{2} (1, -\sqrt{3}). \quad (1.1)$$

Where $a = 2.46 \text{ \AA}$ is the lattice constant. The distance between two carbon atoms, however, is given by $a_{CC} = a/\sqrt{3} = 1.42 \text{ \AA}$. The lattice described above is not a Bravais lattice, since it is not possible to connect A and B with a lattice vector $\mathbf{R} = n_1\mathbf{a}_1 + n_2\mathbf{a}_2$, where n_1 and n_2 are integers. On the other hand, we notice that the lattice only containing the A (or B) atomic positions is indeed a Bravais lattice, i.e. a hexagonal lattice, which we call A sublattice (or B sublattice). Each carbon atom has four valence electrons, one occupying the 2s orbital,

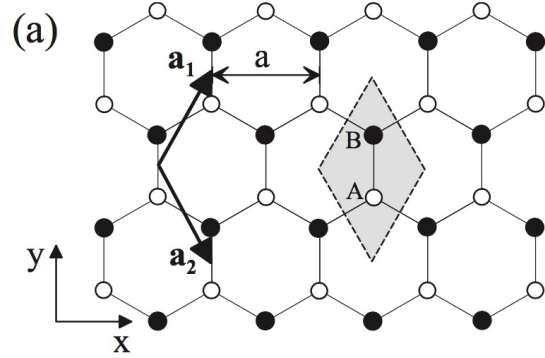


Figure 1.1: Crystal structure of graphene with primitive lattice vectors, grey shaded area denotes a unit cell [5].

the remaining three occupying the $2p_x$, $2p_y$ and $2p_z$ orbital. Similar to graphite the s , p_x and p_y orbitals are hybridized, forming three sp^2 orbitals that lie in the graphene plane and span an angle of 120° between each other. The remaining $2p_z$ orbital rests perpendicular to the plane. It is this orbital that forms the bond between graphene layers in graphite, but since we examine monolayer graphene it remains unbound.

1.2 Tight-Binding Model

We calculate the band structure of graphene, in order to study its electrooptical properties, by applying the tight-binding model. In the general case, we observe a system that consists of N unit cells, each containing n atomic orbitals, which we call ϕ_j ($j = 1 \dots n$). Since we examine a periodic structure, we may introduce a Bloch wave function Φ_j that describes the time evolution of an atomic orbital in not just one unit cell, but our whole solid, i.e. in all N unit cells. It depends on the position \mathbf{r} and the wave vector \mathbf{k} of the electron, \mathbf{R}_{ji} denotes the position of the j th orbital electron in the i th unit cell. It reads

$$\Phi_j(\mathbf{k}, \mathbf{r}) = \frac{1}{\sqrt{N}} \sum_{i=1}^N e^{i\mathbf{k}\mathbf{R}_{ji}} \phi_j(\mathbf{r} - \mathbf{R}_{ji}). \quad (1.2)$$

The electronic wavefunction describing the whole electronic system is a linear superposition of all the distinct orbital wave functions (with complex coefficients c_{jl}):

$$\Psi_j(\mathbf{k}, \mathbf{r}) = \sum_{l=1}^n c_{jl}(\mathbf{k}) \Phi_l(\mathbf{k}, \mathbf{r}). \quad (1.3)$$

The energy of the j th band is then given by

$$E_j(\mathbf{k}) = \frac{\langle \Psi_j | \mathcal{H} | \Psi_j \rangle}{\langle \Psi_j | \Psi_j \rangle} = \frac{\sum_{i,l}^n c_{ji}^* c_{jl} \langle \Phi_i | \mathcal{H} | \Phi_l \rangle}{\sum_{i,l}^n c_{ji}^* c_{jl} \langle \Phi_i | \Phi_l \rangle}, \quad (1.4)$$

where we introduce the matrix elements $H_{ij} = \langle \Phi_i | \mathcal{H} | \Phi_j \rangle$ and $S_{ij} = \langle \Phi_i | \Phi_j \rangle$. \mathcal{H} denotes the Hamiltonian of our system and c_{ji}^* denotes the complex conjugate of c_{ji} . We minimize the energy with respect to the coefficients, which leads to the following equation:

$$\frac{\partial E_j}{\partial c_{jm}^*} = 0 \Rightarrow \sum_{l=1}^n H_{ml} c_{jl} = E_j \sum_{l=1}^n S_{ml} c_{jl}. \quad (1.5)$$

We rewrite Eq. (1.5) in the form

$$\det(H - E_j S) = 0, \quad (1.6)$$

where we introduced

$$H = \begin{pmatrix} H_{11} & \dots & H_{1n} \\ \vdots & \ddots & \vdots \\ H_{n1} & \dots & H_{nn} \end{pmatrix}, \quad S = \begin{pmatrix} S_{11} & \dots & S_{1n} \\ \vdots & \ddots & \vdots \\ S_{n1} & \dots & S_{nn} \end{pmatrix}. \quad (1.7)$$

The matrix H is known as the transfer integral matrix, whereas the matrix S is known as the overlap integral matrix. Solving Eq. (1.6) yields the band structure, i.e. expressions for the energies E_j in terms of the wavevector \mathbf{k} .

In order to describe graphene with the tight-binding model, we have to set up two Bloch waves, one for each of the hexagonal sublattices. Furthermore each of these waves contains only one orbital, the $2p_z$ orbital. If we only take next neighbour coupling into account, the transfer- and overlap integral are given by [5]

$$H = \begin{pmatrix} \epsilon_{2p} & -\gamma_0 f(\mathbf{k}) \\ -\gamma_0 f^*(\mathbf{k}) & \epsilon_{2p} \end{pmatrix}, \quad S = \begin{pmatrix} 1 & -s_0 f(\mathbf{k}) \\ -s_0 f^*(\mathbf{k}) & 1 \end{pmatrix}, \quad (1.8)$$

where the function $f(\mathbf{k})$ describes nearest neighbour hopping, along with the nearest neighbour hopping parameter γ_0 and the nearest neighbour overlap parameter s_0 . ϵ_{2p} denotes the energy of the $2p_z$ orbital.

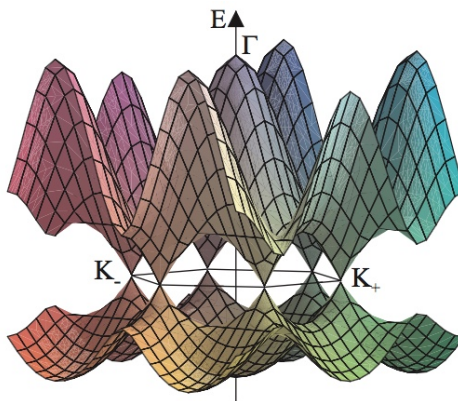


Figure 1.2: Band structure $E(\mathbf{k})$ with parameter values $\epsilon_{2p} = 0$, $\gamma_0 = 3.033$ eV and $s_0 = 0.129$ [5]. Γ denotes the center of the Brillouin zone. The valence and conducting band touch at the so called K points, two of them denoted by K_+ and K_- .

The reader might consider Ref. [5] for the definition of these quantities. It is, however, worth noting that the value of these parameters can not be found within the tight-binding model. We have to use another approach like density-functional theory or find the parameters from comparison with experiments. In any case the energy found reads

$$E_{\pm} = \frac{\epsilon_{2p} \pm \gamma_0 |f(\mathbf{k})|}{1 \mp s_0 |f(\mathbf{k})|}. \quad (1.9)$$

We call E_+ the conduction band and E_- the valence band. The band structure in the vicinity of the first Brillouin zone has been plotted in Fig. 1.2. Two of the corners of the Brillouin zone have been denoted K_+ , K_- respectively and the black line corresponds to ϵ_{2p} , which in this case is set to zero. We can see that the bands touch at the zero energy, leaving no band gap. However, it has been shown in literature that various techniques can be applied to induce a

band gap in graphene, such as placing it above a specific substrate [6]. In Ref. [7] a variety of those findings were concerned, resulting in a range limiting the band gap to

$$\Delta \approx 5 - 50 \text{ meV}. \quad (1.10)$$

On account of this, we may examine graphene inhibiting a nonzero band gap for the following analysis. As a last point, we note that the relation $E(\mathbf{k})$ is linear in the vicinity of the K points.

1.3 Electrooptical Properties

For a linear dispersion, Ref. [5] finds that the Hamiltonian becomes Dirac-like. We therefore assume for all energies a linear dispersion, enabling us to describe graphenes electrooptical response within a (2+1) Dirac model. It depicts the charge carriers in graphene as fermionic quasiparticles moving at the “material speed of light”, which is the Fermi velocity of graphene $v_F \approx \frac{1}{300}c$ (c being the vacuum speed of light). From Section 1.2 we note that the assumption of a linear dispersion only holds for low energies, i.e. for energies in the vicinity of the touching points of the bands. The model is then carried out within a quantum field theoretical calculation, where the so called polarization tensor is coupled to the electromagnetic field, hence giving us the reflection coefficients for graphene. It is a rather involved calculation. The reader might consider Refs. [8–10] for more detail. It is convenient to choose a polarization relative to our system, i.e. where the electric field is parallel to the graphene sheet (TE) or where the magnetic field is parallel to the sheet (TM). The reflections coefficients read

$$r_{\text{TM}} = \frac{\kappa \Pi_{00}}{\kappa \Pi_{00} + 2k^2}, \quad r_{\text{TE}} = \frac{k^2 \Pi_{\text{tr}} - \kappa^2 \Pi_{00}}{k^2 (\Pi_{\text{tr}} + 2\kappa) - \kappa^2 \Pi_{00}}, \quad (1.11)$$

where $k = \sqrt{k_x^2 + k_y^2}$ is the absolute value of the in-plane wavevector, ω is the frequency and $\kappa = \sqrt{k^2 - \omega^2/c^2} = -ik_z$ is connected to the wavevector component perpendicular to the plane. For physical reasons, we consider the definition of the square root, for which $Im[\kappa] < 0$ and note that $Re[\kappa] \geq 0$. Π is the polarization tensor, where Π_{00} denotes the “00” entry and Π_{tr} denotes the trace of the tensor. The polarization tensor is a function of three system parameters: The first one is the temperature T of the system, the second one is the chemical potential μ of the graphene layer, the third one is the band gap Δ of graphene. The latter two represent features that a graphene layer reveals, such as doping ($\mu \neq 0$) or a non-zero band gap ($\Delta \neq 0$). For arbitrary values of these parameters, where the model still holds, the tensor entries have quite long expressions, the reader might find them in Refs. [8–10]. Here we restrict ourselves to the case of an undoped layer of graphene $\mu = 0$ at zero temperature $T = 0$, but with a non-zero band gap $\Delta \neq 0$. For these assumptions the tensor entries have the following form:

$$\Pi_{00} = \alpha \frac{k^2}{\kappa_F^2} \Phi \left(\frac{\kappa_F}{k_\Delta} \right), \quad \Pi_{\text{tr}} = \alpha \frac{\kappa^2 + \kappa_F^2}{\kappa_F^2} \Phi \left(\frac{\kappa_F}{k_\Delta} \right). \quad (1.12)$$

We introduced $\kappa_F = \sqrt{\frac{v_F^2}{c^2} k^2 - \frac{\omega^2}{c^2}} = -ip_F$, $\alpha = \frac{1}{137}$ the fine structure constant and the function

$$\begin{aligned}
\Phi\left(\frac{\kappa_F}{k_\Delta}\right) &= 2k_\Delta \left(1 + \left(\frac{\kappa_F}{k_\Delta} - \frac{k_\Delta}{\kappa_F} \right) \arctan\left(\frac{\kappa_F}{k_\Delta}\right) \right) \\
&= 2k_\Delta \underbrace{\left(1 - \left(\frac{p_F}{k_\Delta} + \frac{k_\Delta}{p_F} \right) \operatorname{arctanh}\left(\frac{p_F}{k_\Delta}\right) \right)}_{:= -\psi\left(\frac{p_F}{k_\Delta}\right)}.
\end{aligned} \tag{1.13}$$

In the following, it is convenient to work with the dimensionless parameters $v_F/c = v$ and $p_F/k_\Delta = p$. The function Φ is real and negative for any value of $0 < p_F/k_\Delta < 1$. The constraint that $p_F < k_\Delta$ is related to no pair creation occurring in the graphene sheets. The expressions of the reflection coefficients also provide us with a set of unit scales for our system, as a function of k_Δ :

$$k_\Delta = \frac{2\Delta}{\hbar c}, \quad \lambda_\Delta = \frac{1}{k_\Delta}, \tag{1.14}$$

where \hbar is the reduced Planck constant. k_Δ has the unit of a wavevector and hence its inverse λ_Δ will serve as the characteristic length of our system, relative to which we call lengths small or large respectively. For the values of the band gap given in Eq. (1.10) we see that $\lambda_\Delta \approx 2 - 20\mu\text{m}$.

We want to end this chapter by stressing the importance of the model with which we describe graphene. It determines the reflection coefficients and therefore influences the Casimir energy, as we will see in Eq. (2.9). An alternative to the Dirac model lies in the possibility to describe the charge carriers in graphene as an incompressible fluid, which is confined to a two dimensional surface. This model is called plasma model and has been applied to a variety of calculations regarding the Casimir effect [11, 12]. However, in Ref. [13] it was shown that, for a certain experimental setup, the plasma model predicts larger magnitudes of the Casimir energy, than the Dirac model does. In Ref. [3] the two models were compared with measurements performed in Ref. [14], with the result that “[...] the theoretical predictions of the plasma model are excluded by the measurement data at a 99% confidence level over a wide region of separations [...]” [3]. The same set of data was shown to be in very good agreement with predictions made using the Dirac model [15]. We therefore conclude that the Dirac model of graphene provides a suitable theoretical description of the Casimir effect within the regime of low energies and justifies its use in the present work.

2 Chapter 2

Casimir Energy

In the beginning of this chapter we present a short overview of the Casimir effect, from its original proposal to its expansion for real materials at nonzero temperatures. In the second part we calculate the Casimir energy of two undoped graphene layers with a nonzero band gap at zero temperature and compare the result to the case of a vanishing band gap.

The Casimir effect is a quantum phenomena where, in its original formulation by H.B.G. Casimir in 1948 [16], two uncharged and perfectly conducting metal plates parallel to each other experience an attracting force obeying

$$\frac{F_{Cas}}{A} = -\frac{\hbar c \pi^2}{240L^4}. \quad (2.1)$$

Here, A is the area of the plates and L is the separation distance. The effect has been confirmed by experiment several times and has inspired a whole field in the physical research known as Casimir physics [17]. A brief description of Casimir's calculation is presented below. The system we consider consists of two parallel and perfectly conducting metallic plates with side length d and separation distance L as shown in Figure 2.1. Possible vibrations in this cavity have the frequencies

$$\omega_{n_x n_y n_z} = c \sqrt{k_x^2 + k_y^2 + k_z^2} = c \sqrt{\frac{\pi^2}{d^2} n_x^2 + \frac{\pi^2}{d^2} n_y^2 + \frac{\pi^2}{L^2} n_z^2}, \quad (2.2)$$

where n_x , n_y and n_z are integers. We now associate every mode in the cavity with a harmonic oscillator in its ground state and perform a sum over all modes

$$E(L) = \sum_{n_x n_y n_z} \frac{\hbar}{2} \omega_{n_x n_y n_z}. \quad (2.3)$$

By assuming $d \gg L$ we can justify that the sum over n_x and n_y becomes an integral, since k_x and k_y become continuous. We note that we have to multiply $E(L)$ with two, since there are two possible polarizations. With $x = \sqrt{k_x^2 + k_y^2}$ and $A = d^2$ we obtain

(the zero at the sum denotes that the zero term has to be multiplied by $\frac{1}{2}$, since there is only one polarization if one n is zero)

$$E(L) = \frac{\hbar c A}{2\pi} \sum_{n=(0)1}^{\infty} \int_0^{\infty} x dx \sqrt{x^2 + \frac{\pi^2}{L^2} n^2}. \quad (2.4)$$

We note that this energy is infinite and now subtract the infinite separation quantity $E_{Cas} = E(L) - E(L \rightarrow \infty)$ from it. In the limit $L \rightarrow \infty$, k_z also becomes continuous. In order to extract the correct limit we have to introduce a regularization, which in this case is a cut-off function

$$f\left(\frac{k}{k_m}\right) = \begin{cases} 1 & k \ll k_m \\ 0 & \frac{k}{k_m} \rightarrow \infty \end{cases}. \quad (2.5)$$

The idea behind it is, that every metal becomes transparent at high enough frequencies, so the function cuts away the parts laying above a certain cut-off frequency. A further substitution ($x^2 = \frac{\pi^2}{L^2} u$) then leads to

$$E_{Cas} = \frac{\hbar c A \pi^2}{4L^3} \left(\sum_{n=(0)1}^{\infty} F(n) - \int_0^{\infty} F(n) dn \right), \quad F(n) = \int_0^{\infty} \sqrt{u + n^2} f\left(\frac{\pi \sqrt{u + n^2}}{L k_m}\right) du. \quad (2.6)$$

We then use the Euler-Maclaurin formula and obtain

$$\frac{E_{Cas}}{A} = -\frac{\hbar c \pi^2}{720 L^3}. \quad (2.7)$$

The resulting force is attractive and is calculated by taking the negative derivative of the energy with respect to L

$$\frac{F_{Cas}}{A} = -\frac{d}{dL} \frac{E_{Cas}}{A} = -\frac{\hbar c \pi^2}{240 L^4}. \quad (2.8)$$

Furthermore, we want to present an argument that becomes particularly interesting for the physical intuition of the effect. The very ground of Casimir's calculation is that he associates every cavity mode with a harmonic oscillator at ground state. He then sums over all the ground-state energies at a finite distance and subtracts the sum of those at infinitely separated plates. In other words, the Casimir effect can be understood as a geometrical phenomenon, where the presence of boundary conditions, i.e. perfectly conducting plates in this case, modifies the ground-state of the vacuum in a way that it induces a macroscopic effect.

Naturally physicists did not stop after the initial calculation and it was for Lifshitz, who

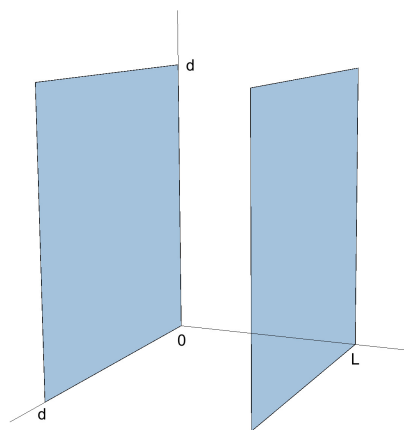


Figure 2.1: *Cavity for the Casimir effect. The side length of the plates is denoted by d , L denotes their separation.*

expanded the theory for dielectric materials and also nonzero temperatures [18]. His approach was more profound than the one Casimir took. He calculated the average of the Maxwell stress tensor inside the cavity, yielding the so called *Lifshitz formula* [9, 10]

$$E_{Cas}(L, T) = \frac{k_B T A}{4\pi} \sum_{n=(0)1}^{\infty} \int_0^{\infty} k dk \left\{ \ln \left[1 - r_{TM}^2(i\xi_n, k) e^{-2\kappa L} \right] + \ln \left[1 - r_{TE}^2(i\xi_n, k) e^{-2\kappa L} \right] \right\}. \quad (2.9)$$

Here $i\xi_n = \frac{2\pi k_B T}{\hbar} n$ are the Matsubara frequencies. The (0) at the sum denotes that we must multiply the $n = 0$ term by $\frac{1}{2}$. The temperature appears as a linear prefactor but also in the Matsubara frequencies. The influence of the material is contained through the reflection coefficients r_{TE} and r_{TM} .

We now want to adjust Eq. (2.9) to our configuration. First we set $T = 0$, so the Matsubara frequencies become continues changing the sum over n to an integral

$$E_{Cas}(L) = \frac{\hbar A}{16\pi^2} \int_0^{\infty} d\xi \int_0^{\infty} k dk \left\{ \ln \left[1 - r_{TM}^2(i\xi, k) e^{-2\kappa L} \right] + \ln \left[1 - r_{TE}^2(i\xi, k) e^{-2\kappa L} \right] \right\}. \quad (2.10)$$

In order to study the behavior of the Casimir energy in terms of the separation distance between the plates, we introduce dimensionless units following the notation of [10].

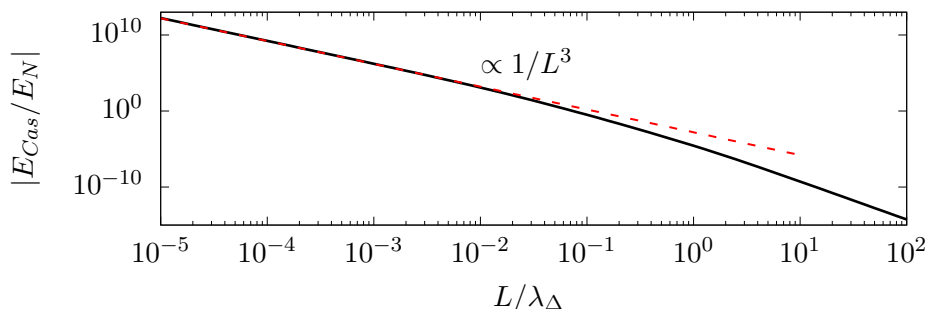


Figure 2.2: Casimir Energy of graphene normalized to $E_N = \frac{\hbar c k_{\Delta}^3 A}{4\pi}$. The (red) dashed line is the expression found in Ref. [10] for a vanishing band gap. In our case it serves as an asymptote for $L \rightarrow 0$.

With $y = 2L\kappa$ and $\zeta = \xi L/c$, we obtain

$$E_{Cas}(L) = \frac{\hbar c A}{32\pi^2 L^3} \int_0^{\infty} y dy \int_0^y d\zeta \left\{ \ln \left[1 - r_{TM}^2(i\zeta, y) e^{-y} \right] + \ln \left[1 - r_{TE}^2(i\zeta, y) e^{-y} \right] \right\}. \quad (2.11)$$

In Ref. [10] it is examined how the Casimir energy acts in the case of a vanishing band gap $\Delta = 0$. There the reflection coefficients do not depend on the separation width L and the

integral in Eq. (2.11) becomes a numerical constant $C = 0.02101$. The Casimir energy can then be written as

$$E_{Cas}(L) = -\frac{\hbar c A}{32\pi^2 L^3} C. \quad (2.12)$$

In our case, however, a non-zero band gap exists and in the new variables the reflection coefficients depend on the separation width via the dimensionless length $\lambda = L/\lambda_\Delta$. We note, however, that for $L \ll \lambda_\Delta$ the reflection coefficients take the same form as in the event of a zero band gap $\Delta = 0$. Therefore, as can be seen in Fig. 2.2, we obtain the same behaviour of the Casimir energy for graphene sheets with a vanishing and a non-vanishing band gap in the limit $L \rightarrow 0$. Furthermore we note that there is no change in the power law of the Casimir energy as a function of the distance L for $\Delta = 0$, similar to the Casimir energy calculated for perfectly conducting plates. For $\Delta \neq 0$, however, we can see in Fig. 2.2 that the power law changes.

3

Chapter 3

Plasmonic Modes Of Graphene

In this chapter we use the reflection coefficients obtained in Chapter 1 to calculate the dispersion relation of the plasmonic modes for both a single layer of graphene and two parallel sheets of graphene. We calculate asymptotic behaviours and compare our results to the literature. The expressions we find will become important for the calculation of the plasmonic part of the Casimir energy in Chapter 4.

3.1 Single Layer Of Graphene

Plasmonic excitations in a material can be described as resonances of its reflection coefficients. In the present thesis we employed the Dirac model described in Chapter 1 to obtain them. For $T = 0$ and $\mu = 0$ the reflection coefficients read

$$r^{TM} = \frac{\alpha\kappa\Phi(p)}{\alpha\kappa\Phi(p) - 2p_F^2}, \quad r^{TE} = -\frac{\alpha\Phi(p)}{\alpha\Phi(p) + 2\kappa}. \quad (3.1)$$

To find the resonances, we have to determine the poles of the reflection coefficients

$$\frac{1}{r} = 0 \Leftrightarrow \begin{cases} \alpha\Phi + 2\kappa = 0 & \text{TE} \\ \alpha\kappa\Phi - 2p_F^2 = 0 & \text{TM} \end{cases}. \quad (3.2)$$

If we regard $\Phi \in \mathbb{R}^-$ and $p_F \in (0, k_\Delta)$ as fixed (see discussion around Eq. (1.13)), the equations (3.2) can be expressed as a function of κ . Reminding the definition of $\kappa = \sqrt{k^2 - \frac{\omega^2}{c^2}}$, possible solutions can be found in the following three domains:

- For $\omega > ck$, κ is complex with a negative imaginary part and a vanishing real part ($\kappa \in -i\mathbb{R}^+$). In this regime the fields propagate, hence we call this domain the *propagating region*
- If $\omega < ck$, κ is a real and positive number ($\kappa \in \mathbb{R}^+$). The fields associated with modes in this region do exponentially decay at the surface, thus we call this domain the *evanescent region*

- The third domain of κ is where $\omega = ck$, such that $\kappa = 0$. This we call the *light cone*, it is the dispersion relation in vacuum.

Now we want to see whether we can find a solution for κ in any of the above regions. Recalling the equation we have to solve for the TM polarization $\alpha\kappa\Phi - 2p_F^2 = 0$ and $\Phi \in \mathbb{R}^-$, $p_F > 0$ we see that the only possible solution would be $\kappa \in \mathbb{R}^-$, which does not match any of the regions mentioned above. Therefore, within our framework, graphene does not exhibit plasmonic excitations in the TM polarization. However there exist solutions for the TE polarization, i.e. one in the evanescent sector. This can be seen by rewriting Eq. (3.2) as

$$2\kappa + \alpha\Phi(p) = 0 \Leftrightarrow \kappa = -\frac{\alpha}{2}\Phi(p) = \alpha k_\Delta \psi(p). \quad (3.3)$$

Unfortunately this equation can't easily (if all) be brought explicitly into the form $\omega = \omega(k)$. One way to circumvent this problem is to express ω and k as functions of a common parameter. Recalling that $pk_\Delta = \sqrt{\frac{\omega^2}{c^2} - v^2k^2}$ and $\kappa = \sqrt{k^2 - \frac{\omega^2}{c^2}}$, we conclude that p can suffice as such a parameter. Furthermore we note that it is also possible to introduce κ as a parameter, which we will show in Section 3.3. For now, we want to find the parametric expressions with the parameter p . We have to use the definitions of p and κ to eliminate ω or k in Eq. (3.3). The dispersion relation for the single layer TE plasmon of graphene then reads

Single Layer Plasmon Mode

$$k(p) = \frac{k_\Delta}{\sqrt{1-v^2}} \sqrt{p^2 + \alpha^2 \psi^2(p)} \quad (3.4a)$$

$$\omega(p) = \frac{ck_\Delta}{\sqrt{1-v^2}} \sqrt{p^2 + \alpha^2 v^2 \psi^2(p)} \quad (3.4b)$$

The parametric expressions Eq. (3.4) are plotted in Fig. 3.1. We first notice that the mode is defined for all real and positive frequencies and wavevectors, meaning that it doesn't decay. Because $v < 1$ we see that $\omega < ck$, so the surface plasmon lies entirely in the evanescent sector. For the physical values of v and α the mode basically looks like two crossing lines at $k = k_\Delta/\sqrt{1-v^2}$ given by the pair creation threshold frequency and the light cone. We plot the quantities in Fig. 3.1 with different values of these parameters to show that the mode is continuous and differentiable for all k . The crossing lines mentioned will also serve as asymptotes of the mode for small or large values of k .

For small k , i.e. $k \ll k_\Delta$ we see that our parameter p has to be small since k and ω are monotonously increasing functions of p . We see that

$$\psi(p) = \left(p + \frac{1}{p} \right) \operatorname{arctanh}(p) - 1 \stackrel{p \rightarrow 0}{\approx} \frac{4}{3} p^2. \quad (3.5)$$

Therefore the second term under the root in Eq. (3.4) can be neglected and we obtain the dispersion relation of the vacuum: $\omega(k) = ck$. Conversely for large k , i.e. $k \gg k_\Delta$ we see that,

since again k and ω are monotonously increasing functions of p , we have to have large values of p . Reminding that $0 < p < 1$, we see that we're approaching the limiting value of $p = 1$. We obtain the upper bound

$$pk_{\Delta} = \sqrt{\frac{\omega^2}{c^2} - v^2 k^2} \xrightarrow{p=1} \omega_{th}(k) = \sqrt{c^2 k_{\Delta}^2 + v_F^2 k^2}, \quad (3.6)$$

which for large values of $k \gg k_{\Delta}/v$ also gets linear $\omega(k) = v_F k$. We note that our results, regarding the TE plasmon coincide with the ones found in Ref. [19]. It is noted there that even though we assumed $T = 0$ and $\Delta \neq 0$ the plasmon found would survive the case of finite temperatures and $\Delta = 0$.

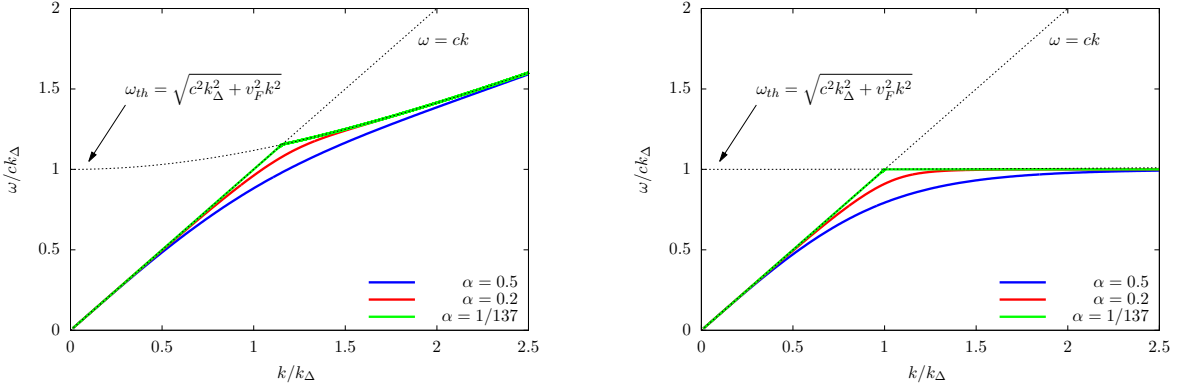


Figure 3.1: Single layer plasmonic mode. Dashed lines are the light cone and the threshold frequency. Different values of fine structure constant α are shown for better visibility, Left pane: $v_F = \frac{1}{2}c$, Right pane: $v_F = \frac{1}{300}c$.

3.2 Two Layers Of Graphene

Let us consider the case of two graphene layers parallel to each other. Each layer supports a TE polarized surface plasmon. At a sufficiently large separation distance the layers do not interact with each other and can be treated as if each layer were isolated. If we, however, bring them ever closer, their individual modes couple in a symmetric (ω_-) and antisymmetric (ω_+) way as illustrated in Fig. 3.2. The symmetric mode results in a binding force, whereas the antisymmetric mode is anti-binding [4]. Mathematically the coupled modes are determined by

$$1 - r^2 e^{-2\kappa L} = 0 \Leftrightarrow r = -\sigma e^{-\kappa L}, \quad (3.7)$$

where $\sigma = 1$ corresponds to the binding mode ω_- and $\sigma = -1$ to the anti-binding mode ω_+ . We may rewrite Eq. (3.7) to

$$\alpha\psi(p) = \begin{cases} \frac{\mu}{1-e^{-\mu\lambda}} = \frac{\mu}{2} \left[1 + \coth\left(\frac{\mu\lambda}{2}\right) \right] = \frac{1}{\lambda} f_+(\mu\lambda) & \sigma = 1 \\ \frac{\mu}{1+e^{-\mu\lambda}} = \frac{\mu}{2} \left[1 + \tanh\left(\frac{\mu\lambda}{2}\right) \right] = \frac{1}{\lambda} f_-(\mu\lambda) & \sigma = -1 \end{cases}, \quad (3.8)$$

where we introduce the dimensionless length $\lambda = L/\lambda_\Delta$ and $\mu = \kappa/k_\Delta$. Similar to the case of a single layer, we regard $\psi \in \mathbb{R}^+$ and $p \in (0, 1)$ as fixed, so the Eqs. (3.8) can be expressed as a function of μ . Possible, physical solutions lie in one of the three domains: *propagating region* ($\mu \in -i\mathbb{R}^+$), *evanescent region* ($\mu \in \mathbb{R}^+$) or *light cone* ($\mu = 0$).

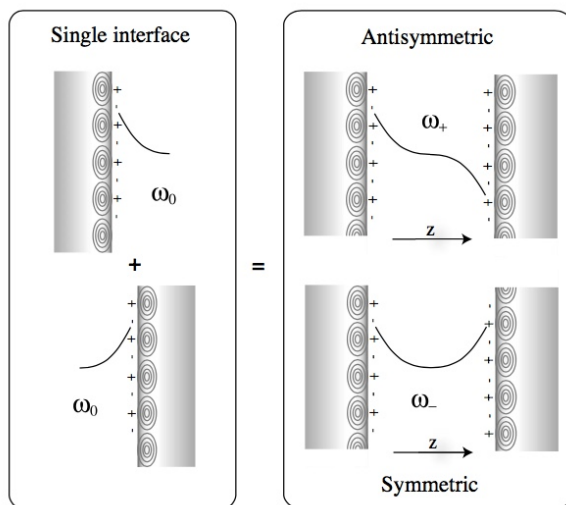


Figure 3.2: Schematic visualization of the modes of two parallel slabs at infinite (left) and finite (right) separation. For infinite separation each slab features a plasmonic mode (ω_0) individually, which couple in a symmetric (ω_-) or antisymmetric fashion (ω_+) [4].

We can see that in the propagating sector we may write $\mu = -ix$, where $x \in \mathbb{R}^+$

$$\mathbb{R}^+ \ni \alpha\psi(p) = \begin{cases} -\frac{ix}{2} \left[1 + \coth\left(-\frac{ix\lambda}{2}\right) \right] = -\frac{ix}{2} + \frac{x}{2} \cot\left(\frac{x\lambda}{2}\right) \in \mathbb{C} \\ -\frac{ix}{2} \left[1 + \tanh\left(-\frac{ix\lambda}{2}\right) \right] = -\frac{ix}{2} - \frac{x}{2} \tan\left(\frac{x\lambda}{2}\right) \in \mathbb{C} \end{cases}. \quad (3.9)$$

For $x \neq 0$ there is a non vanishing imaginary term on the right hand side of Eq. (3.9), so the domain does not match the left hand side. Hence for both coupled modes there can not be any part in the propagating region. Nonetheless there are solutions in the evanescent sector which we obtain by choosing a parametric expression like in the single layer case. The idea is to find an inverse for the function on the right hand side of Eq. (3.8) and operate it on both sides, isolating $\mu(p)$. We rewrite Eq. (3.8) as

$$\mp \lambda \alpha\psi(p) e^{\lambda \alpha\psi(p)} = \lambda (\mu - \alpha\psi(p)) e^{\lambda (\mu - \alpha\psi(p))}. \quad (3.10)$$

The inverse of xe^x is called the Lambert \mathcal{W} function. For a real variable x it has two branches denoted by 0 and -1 , meaning that it is multivalued

$$x = \begin{cases} \mathcal{W}_0(xe^x) & x \geq -1 \\ \mathcal{W}_{-1}(xe^x) & x \leq -1 \end{cases}. \quad (3.11)$$

For our case this means that we have to inspect whether $\lambda(\mu - \alpha\psi(p)) \geq -1$. We insert the right hand sides of Eq. (3.8) for $\alpha\psi(p)$ and arrive at

$$h_{\pm}(\mu) := \mu - \frac{\mu}{1 \mp e^{-\lambda\mu}} \stackrel{?}{\geq} -\frac{1}{\lambda}. \quad (3.12)$$

Choosing a plus in the denominator this is trivially fulfilled, because $\mu > 0$ and $1 + e^{-\lambda\mu} > 1$. For a minus in the denominator, we use L'Hôpital's rule

$$\lim_{\mu \rightarrow 0} h_{-}(\mu) = \lim_{\mu \rightarrow 0} \left(\mu - \frac{\mu}{1 - e^{-\lambda\mu}} \right) = -\frac{1}{1 + \lambda} \geq -\frac{1}{\lambda}. \quad (3.13)$$

Since $h_{-}(\mu)$ is a monotonous increasing function the condition is also true for the minus case. We can therefore invert the right side of Eq. (3.10) and obtain

$$\mu = f_{\pm}(p, \lambda) = \underbrace{\alpha\psi(p)}_{=: f_0(p)} + \underbrace{\frac{1}{\lambda} \mathcal{W}_0(\pm \alpha\lambda\psi(p)e^{-\alpha\lambda\psi(p)})}_{=: g_{\pm}(p, \lambda)}. \quad (3.14)$$

With that we deduce the parametric expressions with the definitions of $\mu k_{\Delta} = \sqrt{k^2 - \frac{\omega^2}{c^2}}$ and $pk_{\Delta} = \sqrt{\frac{\omega^2}{c^2} - v^2 k^2}$

Coupled Plasmon Modes

$$k_{\pm}(p) = \frac{k_{\Delta}}{\sqrt{1 - v^2}} \sqrt{p^2 + f_{\pm}(p)^2} \quad (3.15a)$$

$$\omega_{\pm}(p) = \frac{ck_{\Delta}}{\sqrt{1 - v^2}} \sqrt{p^2 + v^2 f_{\pm}(p)^2} \quad (3.15b)$$

We can see that they are formally similar to the single layer case. Here, however, the functions $f_{\pm} = f_0 + g_{\pm}$ under the square root have a single layer part (f_0) and a part specific to the coupling (g_{\pm}). The expressions in Eq. (3.15) are plotted in Fig. 3.3. We see (analogously to the single layer case) that the coupled modes are defined for all real and positive frequencies and wavevectors, not including any decay. The symmetrically coupled mode is purely evanescent, whereas the antisymmetrically coupled mode features a segment that is evanescent and a segment that coincides with the light cone. Contrary to the single layer mode, the antisymmetrically coupled mode is not differentiable at the point where these two segments meet. From a mathematical point of view this behaviour occurs because of the argument in the Lambert

\mathcal{W} function. We see that in the plus case the argument basically has the form of Eq. (3.11). Indeed the transition can be found at

$$\alpha\lambda\psi(p_{\dagger}) = 1 \Leftrightarrow p_{\dagger} = \psi^{-1}\left(\frac{1}{\alpha\lambda}\right). \quad (3.16)$$

This behavior can be interpreted in terms of a threshold frequency $\omega_{\dagger} = \frac{ck_{\Delta}}{\sqrt{1-v^2}}\sqrt{p_{\dagger}^2 + v^2 f_{\pm}(p_{\dagger})^2}$ that has to be reached to give rise to an antisymmetric plasmon. Interestingly the antisymmetric coupling never results in a propagating field.

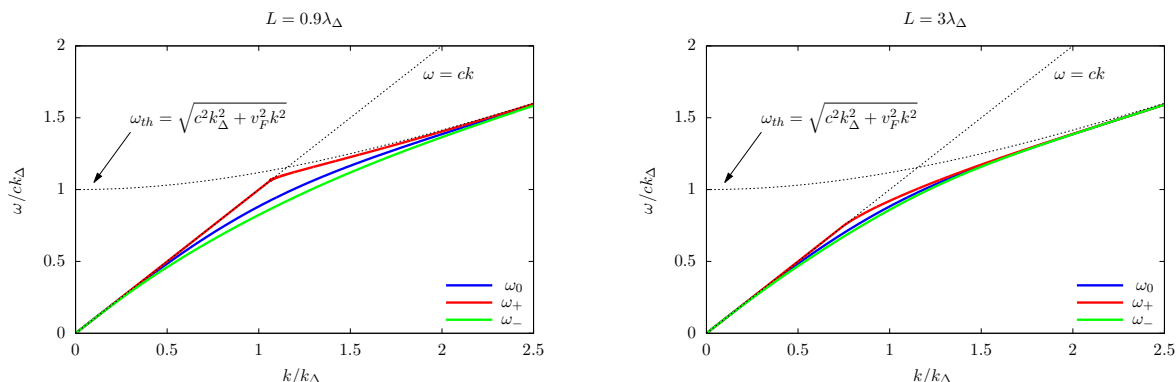


Figure 3.3: Coupled plasmonic modes for different separation distances, where we set $\alpha = v = 1/2$ for better visibility. Dashed lines are the light cone and the threshold frequency.

For small separations $L \ll \lambda_{\Delta}/\alpha\psi(p)$ we can use the Taylor series of the Lambert \mathcal{W} function

$$\mathcal{W}_0(x) \approx x - x^2 + \frac{3}{2}x^3 + \mathcal{O}(x^4) \quad (3.17)$$

and therefore obtain

$$g_{\pm}(p, \lambda \rightarrow 0) = \pm\alpha\psi(p) \mp \alpha^2\lambda\psi^2(p) + \mathcal{O}(\lambda^3). \quad (3.18)$$

Thus, the short distance asymptote of the minus mode becomes

$$k_{-}(p) = \frac{k_{\Delta}}{\sqrt{1-v^2}}\sqrt{p^2 + 4\alpha^2\psi^2(p)}, \quad (3.19a)$$

$$\omega_{-}(p) = \frac{ck_{\Delta}}{\sqrt{1-v^2}}\sqrt{p^2 + 4v^2\alpha^2\psi^2(p)}. \quad (3.19b)$$

Because of Eq. (3.11) the plus mode will always approach the light cone for $L \ll \lambda_{\Delta}/\alpha\psi(p)$. If $L > \lambda_{\Delta}/\alpha\psi(p)$, we can see that p has to get large to still justify the case of small L . For small separations the plus mode therefore approaches the asymptotes of the single layer plasmon for small/large wavevector respectively

$$\omega_+(k) = \begin{cases} ck & k \leq \frac{k_\Delta}{\sqrt{1-v^2}} \\ \sqrt{c^2 k_\Delta^2 + v_F^2 k^2} & k \geq \frac{k_\Delta}{\sqrt{1-v^2}} \end{cases}. \quad (3.20)$$

For large separations $L \rightarrow \infty$ we can see that the coupling specific part g_\pm can be written in the following form (with $x = \alpha\lambda\psi(p)$)

$$\lim_{x \rightarrow \infty} g_\pm(x) = \lim_{x \rightarrow \infty} \alpha\psi(p) \frac{1}{x} \mathcal{W}_0(\pm x e^{-x}) = \alpha\psi(p) \lim_{x \rightarrow \infty} \frac{\mathcal{W}_0(\pm x e^{-x})}{1 + \mathcal{W}_0(\pm x e^{-x})} \left(1 - \frac{1}{x}\right) = 0, \quad (3.21)$$

where we used L'Hôpital's rule and $\mathcal{W}_0(0) = 0$. Therefore, both modes tend to the single layer mode for very large separations. This is exactly what we expected, because for infinite separations the modes of the two plates decouple, leaving two single layer interfaces.

3.3 Parametrization

In the previous section, we found parametric expressions for the coupled plasmons with the parameter p . We therefore took the inverse of the right-hand side of Eq. (3.8) to isolate μ and then used the connection of p and μ with k and ω , obtaining the parametric expressions. We might as well could have taken the inverse of the left side, isolating p and using μ as a parameter. Taking the inverse of ψ and again using $pk_\Delta = \sqrt{\frac{\omega^2}{c^2} - v^2 k^2}$ we get

$$k_\pm(\mu, \lambda) = k_\Delta \sqrt{\mu^2 + \psi^{-1} \left(\frac{f_\pm(\mu\lambda)}{\alpha\lambda} \right)^2}, \quad (3.22a)$$

$$\omega_\pm(\mu, \lambda) = ck_\Delta \sqrt{v^2 \mu^2 + \psi^{-1} \left(\frac{f_\pm(\mu\lambda)}{\alpha\lambda} \right)^2}. \quad (3.22b)$$

There are some small disadvantages in choosing this parametrization instead of the one found in the previous section. One is that the inverse functions can not be written in an analytical form. Another one is that they do not automatically inhibit the analytical continuation to the light cone as the p parametrisation does. We therefore have to “manually” continue the plus mode with the light cone. The modes described by these parametric expressions is of course the same as already elucidated in Chapter 3. Naturally the parameter we choose must not change the physics. It becomes useful to write $p = \tanh(q)$ with $q \in \mathbb{R}^+$ to get

$$\psi(p) = \chi(q) = \left(\tanh(q) + \frac{1}{\tanh(q)} \right) q - 1 = \eta(2q) - 1, \quad (3.23)$$

where we defined $\eta(x) = x \coth(x)$ and note

$$\eta(x \lesssim 1) \approx 1 + \frac{x^2}{3} + \mathcal{O}(x^3), \quad \eta(x > 1) \approx x + \mathcal{O}(e^{-2x}). \quad (3.24)$$

Now we can write the inverse as:

$$\psi^{-1}\left(\frac{f_{\pm}(\mu\lambda)}{\alpha\lambda}\right) = \tanh\left(\chi^{-1}\left[\frac{f_{\pm}(\mu\lambda)}{\alpha\lambda}\right]\right) = \tanh\left(\frac{1}{2}\eta^{-1}\left[1 + \frac{f_{\pm}(\mu\lambda)}{\alpha\lambda}\right]\right). \quad (3.25)$$

This matryoshka-like nesting of functions will become useful in the next chapter, where we'll calculate asymptotes for the plasmonic energy.

4 Chapter 4

Plasmonic Energy

In this chapter we investigate the contribution of plasmonic modes to the Casimir energy by isolating the plasmonic part of the Casimir energy, which we call the plasmonic energy and calculate asymptotes for the limit of very small and very large separations.

We introduced the Casimir energy in Chapter 2 as a sum over modes. From this point of view one might divide this sum into parts including specific modes [4, 12]

$$E_{Cas} = E_{pl} + E_{ph}, \quad (4.1)$$

where E_{pl} contains the plasmonic modes and E_{ph} contains the photonic modes. For observing the contribution of plasmonic modes we isolate the obtained modes in a quantity we call the *plasmonic energy*

$$E_{pl} = \sum_{\mathbf{k}} \left[\frac{\hbar\omega_+}{2} + \frac{\hbar\omega_-}{2} \right]_{L \rightarrow \infty}^L, \quad (4.2)$$

where ω_+ and ω_- are the (anti-)symmetrically coupled plasmonic modes we calculated in Section 3.2. The limit $L \rightarrow \infty$ may be evaluated by subtracting two times the single layer plasmonic mode, since in this limit the interfaces decouple, forming two non interacting layers (see discussion in Section 3.2). We rewrite the sum as an integral

$$E_{pl} = \frac{\hbar}{2} \sum_{\mathbf{k}} \omega_+ + \omega_- - 2\omega_0 \quad (4.3)$$

$$= \frac{\hbar A}{4\pi} \int_0^\infty k dk (\omega_+ + \omega_- - 2\omega_0), \quad (4.4)$$

where k is the radius of an in-plane wavevector with coordinates (k_x, k_y) . We introduce dimensionless units through $K = k/k_\Delta$ and $\Omega_i = \omega_i/c k_\Delta$ ($i = +, -, 0$) and obtain

Plasmonic Energy

$$E_{pl} = E_N \int_0^\infty K dK (\Omega_+ + \Omega_- - 2\Omega_0) \quad (4.5)$$

The prefactor $E_N = \frac{\hbar c k_\Delta^3 A}{4\pi}$ has the unit of an energy and we use it as a normalization constant. We now want to insert the parametric expressions found in Section 3.3, where we express K and Ω_i as functions of a parameter μ . This particular parametrization has the disadvantage, that it does not feature the analytical continuation of the plus mode.

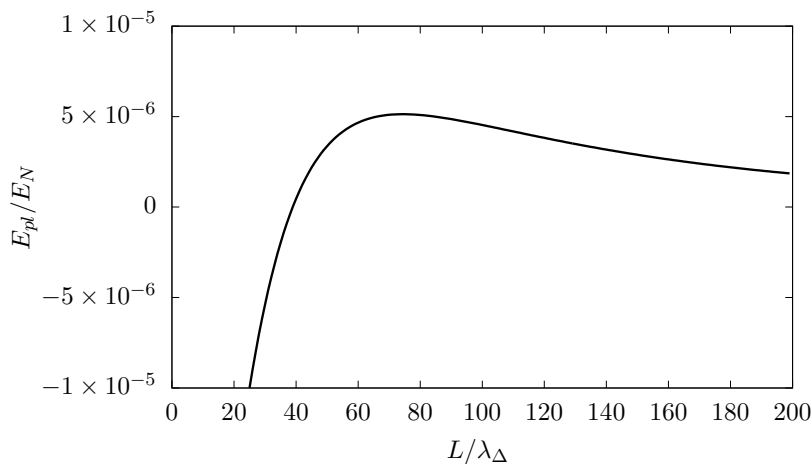


Figure 4.1: Plasmonic Energy for physical values $\alpha = 1/137$ and $v = 1/300$ as a function of the dimensionless length $\lambda = L/\lambda_\Delta$.

We have to write the integral over it like

$$\int_0^\infty K dK \Omega_+ = \int_{K_\dagger}^\infty K dK \Omega_+(\mu, \lambda) + \int_0^{K_\dagger} K^2 dK, \quad (4.6)$$

where K_\dagger is the value at which the propagating region changes to the light cone. We change the integration variable to μ , obtaining

$$K^2 = \mu^2 + \Omega^2 \Rightarrow K dK = \mu d\mu + \Omega d\Omega. \quad (4.7)$$

The Eq. (4.5) then read

$$E_{pl}/E_N = \frac{1}{3} \left[\Omega_+^3 \right]_{K \rightarrow K_\dagger}^{K \rightarrow \infty} + \frac{1}{3} \left[\Omega_-^3 - 2\Omega_0^3 \right]_{K \rightarrow 0}^{K \rightarrow \infty} + \int_{\Gamma_{+,-,0}} [\Omega_+ + \Omega_- - 2\Omega_0] \mu d\mu + \frac{1}{3} K_\dagger^3, \quad (4.8)$$

where $\Gamma_{+,-,0}$ is the integration path. The upper limits of the first two terms of the previous expression cancel, since in this limit the modes tend to a common value (see discussion around

Eq. (3.21)). For the lower limit we know that the zero and minus mode vanish, since they are approaching the light cone. Thus we are left with the lower limit of the plus mode, which cancels the last term in Eq. (4.8). The range of our parameter is $\mu \in \mathbb{R}^+$ and determines the integration paths, leading to

$$E_{pl}/E_N(\lambda) = \int_0^\infty [\Omega_+(\mu, \lambda) + \Omega_-(\mu, \lambda) - 2\Omega_0(\mu)] \mu d\mu. \quad (4.9)$$

Figure 4.1 shows a plot of Eq. (4.9), where we can see that the plasmonic energy monotonously increases until a maximum at $L_{max} \approx 74\lambda_\Delta$. It then decreases monotonously and approaches zero for $L \rightarrow \infty$. We will analyze these limits analytically below. First, it is interesting to understand the physical meaning of our result. Since the Casimir force is the negative derivative of the Casimir energy, we find the part of the force which plasmons cause in the Casimir effect by observing the slope of the plasmonic energy. We see that up to L_{max} the contribution to the force, from the surface plasmon, is attractive. It then changes sign and becomes repulsive for $L > L_{max}$.

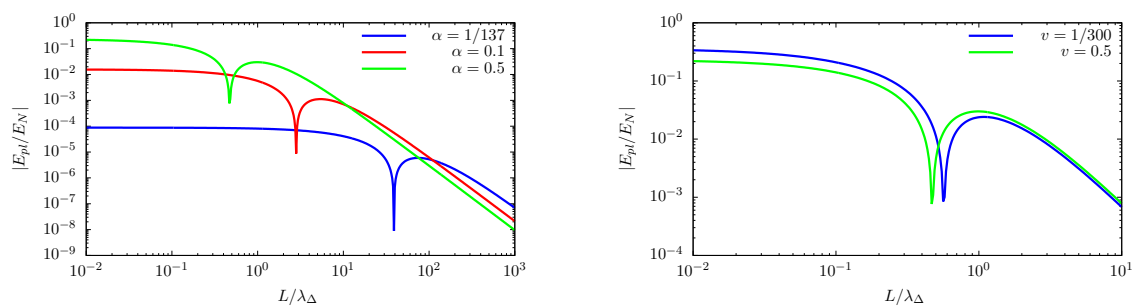


Figure 4.2: Plasmonic Energy for various parameters. Left pane: Fixed value of $v = 1/2$, Right pane: Fixed value of $\alpha = 1/2$. The peak occurs, because we plot the absolute value of E_{pl} .

In Fig. 4.2 the plasmonic energy is plotted with different values of its parameters. We see that the exact value of the dimensionless Fermi velocity v and the fine structure constant α does not change the qualitative behaviour of the plasmonic energy, although it changes the magnitude and the exact position of the maximum.

We now want to analytically analyze the asymptotic behaviour of the plasmonic energy for small and large separations between the graphene sheets. It becomes useful to examine the difference between the coupled and the uncoupled mode, which reads

$$\omega_{\pm}(\mu, \lambda) - \omega_0(\mu) = \frac{ck_{\Delta}}{\sqrt{1-v^2}} \left[\sqrt{v^2\mu^2 + \psi^{-1} \left(\frac{f_{\pm}(\mu\lambda)}{\alpha\lambda} \right)^2} - \sqrt{v^2\mu^2 + \psi^{-1} \left(\frac{f_0(\mu\lambda)}{\alpha\lambda} \right)^2} \right]. \quad (4.10)$$

The largest contribution of this expression occurs at $\mu \approx \alpha$, which can be checked by a plot. Involving that $v < 1$ and $\alpha < 1$ we see that the first term under the square root is negligible

compared to the second. We then insert the inverse function as shown in Eq. (3.25). We approximate $\eta^{-1}(x) \approx x$, so our intermediary result is

$$\omega_{\pm}(\mu, \lambda) - \omega_0(\mu) = \frac{ck_{\Delta}}{\sqrt{1-v^2}} \left[\tanh \left[\frac{1}{2} \left(1 + \frac{f_{\pm}(\mu\lambda)}{\alpha\lambda} \right) \right] - \tanh \left[\frac{1}{2} \left(1 + \frac{f_0(\mu\lambda)}{\alpha\lambda} \right) \right] \right]. \quad (4.11)$$

At $\mu \approx \alpha$ we approximate $\tanh(x) \approx 1 - 2e^{-2x}$. Therefore, we get

$$\omega_{\pm}(\mu, \lambda) - \omega_0(\mu) = \frac{2ck_{\Delta}}{e\sqrt{1-v^2}} \left[\exp \left[-\frac{f_0(\mu\lambda)}{\alpha\lambda} \right] - \exp \left[-\frac{f_{\pm}(\mu\lambda)}{\alpha\lambda} \right] \right], \quad (4.12)$$

where e is Euler's number. For $L \ll \lambda_{\Delta}/\alpha$ the argument of f_0 and f_{\pm} becomes very small. We note that

$$f_{+}(x \rightarrow 0) = f_0(x) + 1 - \frac{x}{2} + \frac{x^2}{12} + \mathcal{O}(x^3), \quad f_{-}(x \rightarrow 0) = f_0(x) - \frac{x}{2} + \frac{x^2}{4} + \mathcal{O}(x^3). \quad (4.13)$$

Recalling that $f_0(x) = x$, we may write

$$\omega_{\pm}(\mu, \lambda) - \omega_0(\mu) = \frac{2ck_{\Delta}}{e\sqrt{1-v^2}} \exp \left[-\frac{\mu}{\alpha} \right] \left\{ 1 - \exp \left[\frac{f_0(\mu\lambda) - f_{\pm}(\mu\lambda)}{\alpha\lambda} \right] \right\}. \quad (4.14)$$

Inserting this expression back into the plasmonic energy given by Eq. (4.5) we find

$$E_{pl}/E_N = \frac{2}{e\sqrt{1-v^2}} \int_0^{\infty} \mu d\mu \exp \left[-\frac{\mu}{\alpha} \right] \left\{ 2 - \exp \left[\frac{\mu}{2\alpha} \left(1 - \frac{\mu\lambda}{2} \right) \right] - \exp \left[\frac{\mu}{2\alpha} \left(1 - \frac{2}{\mu\lambda} - \frac{\mu\lambda}{6} \right) \right] \right\} \quad (4.15)$$

The integral has a rather long, but nonetheless analytical form. For $L \rightarrow 0$ we can further approximate it, so that the plasmonic energy becomes

$$E_{pl}(L \rightarrow 0)/E_N \approx \frac{1}{e\sqrt{1-v^2}} (-4\alpha^2 + 48\alpha^3\lambda - \mathcal{O}(\lambda^2)). \quad (4.16)$$

We see that, in this limit, the plasmonic energy approaches a constant, which can also be seen in Fig. 4.3. We note that the asymptote slightly deviates from the full result. It is likely that this occurs because the approximation of the inverse function ($\eta^{-1}(x) \approx x$) requires more care. This point will be further investigated in future work. As a comparison we note the results found in Ref. [12]. There the Casimir interaction between two plasma sheets was considered, which, generally speaking, could also be used as a model for describing graphene. It was concluded, that the contribution to the Casimir energy stemming from surface plasmons behaves for all distances like $\propto 1/L^{5/2}$, while the whole interaction behaves like $\propto 1/L^3$. Thus,

in that framework it was concluded, that plasmons dominate the near separation limit. Within our treatment however, we have shown, that if we describe graphene with the Dirac model, the plasmonic contribution is negligible at small distances with respect to the total (diverging) interaction.

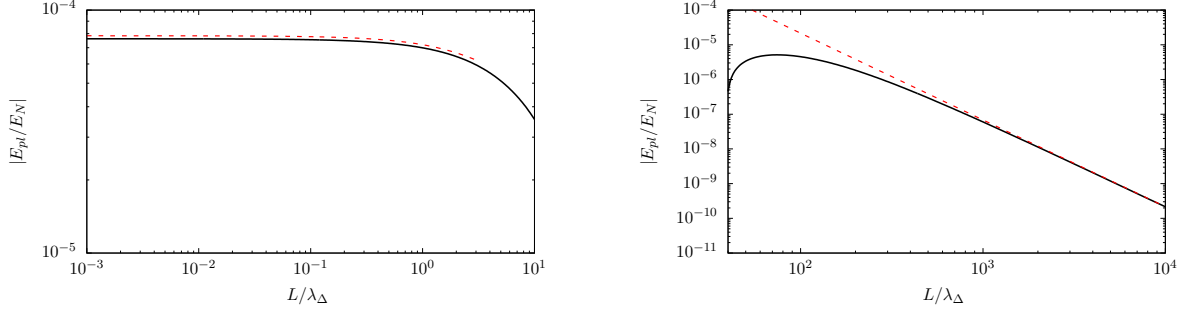


Figure 4.3: Plasmonic energy in different limits with asymptotes (red dashed) for the physical values $v = 1/300$ and $\alpha = 1/137$. Left pane: $L \rightarrow 0$, Right pane: $L \rightarrow \infty$

We now study the plasmonic energy at large distances, i.e. $L \rightarrow \infty$ and again observe the difference between the coupled and the uncoupled mode

$$\omega_{\pm}(\mu, \lambda) - \omega_0(\mu) = \frac{ck_{\Delta}}{\sqrt{1-v^2}} \left[\sqrt{v^2\mu^2 + \psi^{-1} \left(\frac{f_{\pm}(\mu\lambda)}{\alpha\lambda} \right)^2} - \sqrt{v^2\mu^2 + \psi^{-1} \left(\frac{f_0(\mu\lambda)}{\alpha\lambda} \right)^2} \right]. \quad (4.17)$$

Now the largest contributions arise from $\mu \approx 1/\lambda$ and again we can see, that we can neglect the first term in our square root. Furthermore we can approximate the η^{-1} function for arguments around 1 with $\eta^{-1}(x) \approx \sqrt{3(x-1)}$ and we also note for $x \approx 0$: $\tanh(x) \approx x$. The expression now reads

$$\omega_{\pm}(\mu, \lambda) - \omega_0(\mu) = \frac{\sqrt{3}ck_{\Delta}}{2\sqrt{1-v^2}} \left[\sqrt{\frac{f_{\pm}(\mu\lambda)}{\alpha\lambda}} - \sqrt{\frac{f_0(\mu\lambda)}{\alpha\lambda}} \right]. \quad (4.18)$$

Inserting this into the plasmonic energy integral we obtain

$$E_{pl}/E_N = \sqrt{\frac{3}{4\alpha(1-v^2)}} \int_0^{\infty} \mu d\mu \left[\sqrt{\frac{\mu}{2} \left(1 + \tanh \left(\frac{\mu\lambda}{2} \right) \right)} + \sqrt{\frac{\mu}{2} \left(1 + \coth \left(\frac{\mu\lambda}{2} \right) \right)} - 2\sqrt{\mu} \right]. \quad (4.19)$$

We introduce the variable $x = \mu\lambda$ and see that the plasmonic energy takes the form:

$$E_{pl}/E_N = \sqrt{\frac{3}{4\alpha(1-v^2)}} \frac{C}{\lambda^{5/2}} \quad (4.20)$$

Where C is a constant defined by:

$$C = \int_0^\infty x dx \left[\sqrt{\frac{x}{2} \left(1 + \tanh\left(\frac{x}{2}\right) \right)} + \sqrt{\frac{x}{2} \left(1 + \coth\left(\frac{x}{2}\right) \right)} - 2\sqrt{x} \right] \approx 0.2132 \quad (4.21)$$

A plot of this asymptote can be seen in Fig. 4.3. We conclude that plasmons contribute to the Casimir energy at large distance in a repulsive fashion, which is balanced out by the photonic modes to recover the attractive behaviour of the whole Casimir force. Our results are similar to those found for a plasma confined to a two dimensional surface in Ref. [12].

5

Chapter 5

Summary

We introduced graphene theoretically and described its electrooptical behaviour in a (2+1) Dirac model, where we outlined the differences compared to the plasma model. We then calculated the Casimir energy for two undoped sheets of graphene at zero temperature with a nonzero band gap. For small separation distances we recover the already found results for a graphene system with a vanishing band gap [10] and for larger distances we observed a change in the power law of the Casimir energy. We then proceeded by calculating the plasmonic excitations in a single layer of graphene and found out that there only exists one in the TE polarization. For two coupled layers the interaction gives rise to two surface plasmons, which are characterized by an evanescent field. Using these results, we calculated the contribution of the plasmonic modes to the Casimir energy. For small distances between the graphene layers, the whole Casimir energy is negatively diverging, while we showed that the plasmonic Casimir energy approaches a constant in this limit. We concluded that, in the Casimir interaction between two graphene layers, plasmonic modes do not dominate the near separation limit, contrary to what has been found in literature [12], where graphene has been described by the plasma model. For large distances, however, we obtain the same power law as received from the plasma model.

Bibliography

1. D. K. Shaeffer, “MEMS inertial sensors: A tutorial overview”, *IEEE Communications Magazine* **51**, 100 (2013).
2. K. S. Novoselov *et al.*, “Electric Field Effect in Atomically Thin Carbon Films”, *Science* **306**, 666 (2004).
3. G. L. Klimchitskaya and V. M. Mostepanenko, “Comparison of hydrodynamic model of graphene with recent experiment on measuring the Casimir interaction”, *Phys. Rev. B* **91**, 045412 (2015).
4. F. Intravaia, C. Henkel and A. Lambrecht, “Role of surface plasmons in the Casimir effect”, *Phys. Rev. A* **76**, 033820 (2007).
5. E. McCann. *Graphene Nanoelectronics: Metrology, Synthesis, Properties and Applications* (ed H. Raza) 237 (Springer Berlin Heidelberg, Berlin, Heidelberg, 2012).
6. G. Giovannetti, P. A. Khomyakov, G. Brocks, P. J. Kelly and J. van den Brink, “Substrate-induced band gap in graphene on hexagonal boron nitride: Ab initio density functional calculations”, *Phys. Rev. B* **76**, 073103 (2007).
7. J. F. M. Werra, F. Intravaia and K. Busch, “TE resonances in graphene-dielectric structures”, *Journal of Optics* **18**, 034001 (2016).
8. I. V. Fialkovsky, V. N. Marachevsky and D. V. Vassilevich, “Finite-temperature Casimir effect for graphene”, *Phys. Rev. B* **84**, 035446 (2011).
9. M. Chaichian, G. L. Klimchitskaya, V. M. Mostepanenko and A. Tureanu, “Thermal Casimir-Polder interaction of different atoms with graphene”, *Phys. Rev. A* **86**, 012515 (2012).
10. G. L. Klimchitskaya and V. M. Mostepanenko, “van der Waals and Casimir interactions between two graphene sheets”, *Phys. Rev. B* **87**, 075439 (2013).
11. G. Barton, “Casimir effects for a flat plasma sheet: I. Energies”, *Journal of Physics A: Mathematical and General* **38**, 2997 (2005).
12. M. Bordag, “The Casimir effect for thin plasma sheets and the role of the surface plasmons”, *Journal of Physics A: Mathematical and General* **39**, 6173 (2006).
13. M. Bordag, G. L. Klimchitskaya and V. M. Mostepanenko, “Thermal Casimir effect in the interaction of graphene with dielectrics and metals”, *Phys. Rev. B* **86**, 165429 (2012).
14. A. A. Banishev *et al.*, “Measuring the Casimir force gradient from graphene on a SiO₂ substrate”, *Phys. Rev. B* **87**, 205433 (2013).

15. G. L. Klimchitskaya, U. Mohideen and V. M. Mostepanenko, “Theory of the Casimir interaction from graphene-coated substrates using the polarization tensor and comparison with experiment”, *Phys. Rev. B* **89**, 115419 (2014).
16. H. B. G. Casimir, “On the Attraction Between Two Perfectly Conducting Plates”, *Indag. Math.* **10**, 261 (1948).
17. S. Lamoreaux, “Casimir forces: Still surprising after 60 years”, *Physics Today* **60**, 2, 40 (2007).
18. E. M. Lifshitz, “The theory of molecular attractive forces between solids”, *Sov. Phys. JETP* **2**, 73 (1956).
19. M. Bordag and I. G. Pirozhenko, “Transverse-electric surface plasmon for graphene in the Dirac equation model”, *Phys. Rev. B* **89**, 035421 (2014).